C. R. Physique 11 (2010) 316–325

Contents lists available at ScienceDirect

Comptes Rendus Physique

www.sciencedirect.com

Computational metallurgy and changes of scale / Métallurgie numérique et changements d'échelle

Advances in cleavage fracture modelling in steels: Micromechanical, numerical and multiscale aspects

Vers une meilleure compréhension de la rupture par clivage dans les aciers : Aspects micro-mécaniques, numériques et multi-échelles

André Pineau [a,*], Benoît Tanguy [b]

[a] *Centre des matériaux, UMR CNRS 7633, Mines-ParisTech, 91003 Evry cedex, France*
[b] *Département des matériaux pour le nucléaire, CEA Saclay, 91191 Gif-sur-Yvette, France*

ARTICLE INFO

Article history:
Available online 23 August 2010

Keywords:
Cleavage fracture
Micromechanisms
Ferritic steels
Statistics
Scatter
Multiscale modelling

Mots-clés :
Rupture par clivage
Micromécanismes
Aciers ferritiques
Aspects statistiques
Dispersion
Modélisation multi-échelle

ABSTRACT

Brittle cleavage fracture remains one of the major concerns for structural integrity assessment. The main characteristics of this mode of failure in relation to the stress field ahead of a crack, tip are described in the introduction. The emphasis is laid on the physical origins of scatter and the size effect observed in ferritic steels. It is shown that cleavage fracture is controlled by physical events occurring at different scales: initiation at (sub)micrometric particles, propagation across grain boundaries (10–50 microns) and final fracture at centimetric scale. The two first scales are detailed in this paper. The statistical origin of cleavage is described quantitatively from both microstructural defects and stress–strain heterogeneities due to crystalline plasticity at the grain scale. Existing models are applied to the prediction of the variation of Charpy fracture toughness with temperature.

RÉSUMÉ

La ruine par rupture fragile reste une des préoccupations majeures pour l'évaluation de l'intégrité mécanique des structures. Les principaux traits de l'amorçage de ce mode de rupture à la pointe d'une fissure macroscopique sont tout d'abord rappelés dans l'introduction. On met l'accent sur la dispersion inhérente à ce mode de rupture en relation avec l'origine diverse des sites d'amorçage ainsi que sur l'effet de taille. On montre que la rupture par clivage est contrôlée par des mécanismes physiques agissant à différentes échelles, celle des particules de seconde phase micrométriques et celle des grains. L'origine statistique du clivage est modélisée en prenant en compte à la fois la distribution spatiale des défauts microstructuraux et la distribution intragranulaire des contraintes et déformations. Les modèles développés sont utilisés pour prévoir la variation de la résilience avec la température.

* Corresponding author.
E-mail address: andre.pineau@ensmp.fr (A. Pineau).

1631-0705/$ – see front matter
doi:10.1016/j.crhy.2010.07.013

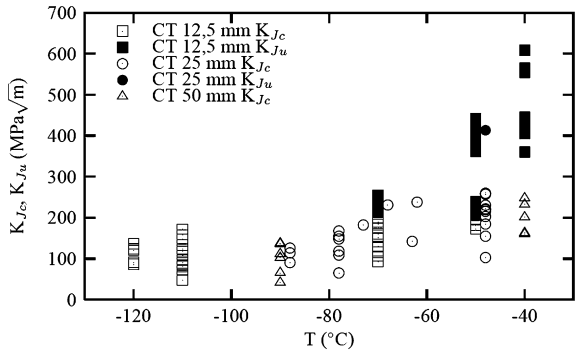

Fig. 1. Illustration of the scatter and of the size effect for the fracture toughness of a pressure vessel steel [2]. CTX: Compact tension specimen with a thickness X (in mm).

Fig. 1. Illustration de la dispersion et de l'effet de taille sur la ténacité d'un acier utilisé pour la fabrication des réacteurs à eau sous pression [2]. CTX : Eprouvette «*Compact Tension*» ayant une épaisseur X (en mm).

1. Introduction

Prevention against brittle cleavage fracture remains one of the major concerns for structural integrity assessment. In most industrial applications the assessment of the mechanical integrity of structures, in particular flawed mechanical structures, relies on the application of linear elastic fracture mechanics (LEFM) developed in the 1950s and on the elastic plastic fracture mechanics (EPFM) developed in the 1970s. These "global" engineering approaches which assume that brittle fracture can be described by a single (or two) parameter(s), such as the stress intensity factor, K_{IC}, or the contour integral, J_{IC}, have remained essentially empirical. However, more recently, since the 1980s new methodologies which are called "local approaches to fracture" (LAF) have been introduced. The first aim of the present paper is to present an overview of these new methodologies which are based on the investigation of the micromechanisms at a local scale and, through a multiscale approach, on the transfer of this local information to the macroscale. More details can be found elsewhere [1]. The final goal is to develop predictive approaches which can be used in finite element codes for structural analysis.

The main characteristics of brittle cleavage fracture are: (i) the scatter (see Fig. 1); (ii) the size effect: fracture toughness decreases when the specimen size is increased (see Fig. 1); (iii) the temperature and loading rate dependence: fracture toughness is an increasing function of temperature (Fig. 1) and a decreasing function of loading rate; (iv) the geometrical dependence: fracture toughness is not an intrinsic property, but is dependent on the geometry of the specimens (this aspect related to pure mechanical conditions is not dealt with in the present paper); and (v) the extreme sensitivity to metallurgical details which is more central in this article.

Engineers usually represent the fracture toughness in terms of the stress intensity factor ($K \approx \sigma\sqrt{\pi a}$), where σ is the applied stress and a the crack length). LEFM tells us that this quantity can be related to the strain energy release rate, G_{Ic} ($G_{\mathrm{Ic}} \sim K_{\mathrm{Ic}}^2/E$) which, as an energy, is more familiar to the physicists. The values reported in Fig. 1, for instance 50 MPa $\mathrm{m}^{0.5}$, lead to a value of G_{Ic} of the order of 10 kJ/m^2. This value is thus much larger by at least 3 orders of magnitude than the surface energy in iron which is of the order of 2–6 J/m^2. In iron, taking Young's modulus to be 200 GPa, surface energy to be 2 J/m^2, and a typical fracture stress, σ_{F}, to be some 1 GPa, we have for the critical flaw size, a_{crit}, a value of 0.1 μm. Pure irons may be made which do not contain inherent, atomically sharp crack as large as 0.1 μm and yet which cleave at low fracture stresses when they are tested at low temperatures. Many experiments have shown that cleavage fracture is always preceded by a small amount of local yielding. This means that the simple relation $G \sim K^2/E$ which is strictly valid for linear elastic behaviour does not strictly apply. In materials like pure irons, brittle fracture is controlled by the initiation and the growth of cracks nucleated from dislocations [3,4] or mechanical twins [5,6]. In these pure materials these two main stages of fracture must be distinguished. In particular the fracture stress, σ_{c}, is temperature dependent (see e.g. [6]), which is not the case in structural steel in which σ_{c} is independent of temperature, at least within a first approximation. This means that is these steels, which are the materials considered in the present paper, fracture is initiated from carbides [6–8] and, in many situations, is essentially "growth controlled".

During its propagation, a nucleated microcrack encounters several microstructural barriers. The crossing of these barriers contributes to the increase of the dissipated energy inherent to fracture process. The role of these microstructural barriers largely explains the differences which can be found when a comparison is made between different steels for reactor pressure vessel (RPV), like 16MND5 and $2^{1/4}$Cr–1Mo steel (see Fig. 2a). This latter material contains a much larger number of high angle grain boundaries than the first steel [9,10]. The role of grain boundaries on brittle cleavage fracture is discussed in more details in the following.

The objective of the present article is to show how the LAF can be used to model the fracture toughness in the brittle cleavage regime. It is well to remember that, due to plasticity and crack tip blunting effect, the highest local stresses in the fracture process zone are not located at the crack tip but at some distance from the tip ($\sim 2 \times$ CTOD) where the CTOD is the crack tip opening displacement; CTOD $\sim K^2/E\sigma_0$, where σ_0 is the yield strength of the material. This situation is illustrated

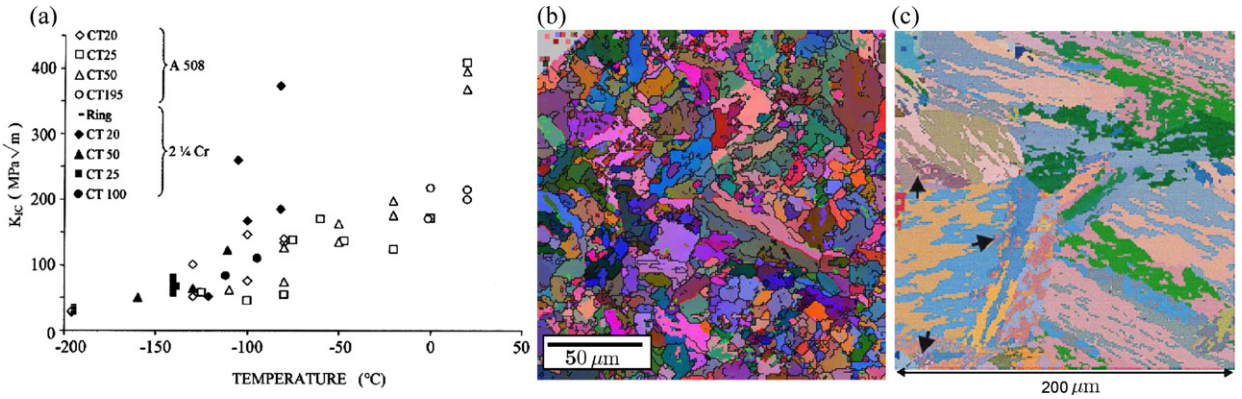

Fig. 2. Fracture toughness properties (a) and crystallographic orientations of two bainitic steels: (b) 16MND5 (A508) with an upper bainite microstructure and (c) $2^{1/4}$Cr–1Mo steel with a lower bainite microstructure [9,10].

Fig. 2. Ténacité de deux aciers bainitiques (a) et orientations cristallographiques de ces aciers : (b) acier 16MND5 (ou A 508) de structure bainitique supérieure et (c) acier $2^{1/4}$Cr–1Mo avec une structure bainitique inférieure [9,10].

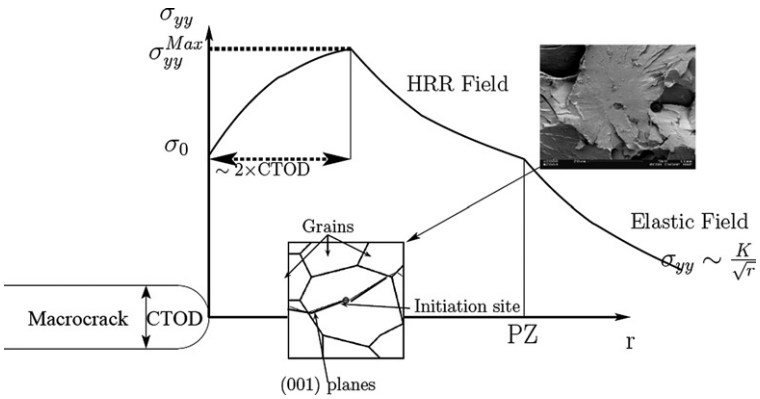

Fig. 3. Schematic representation of the variation of the tensile stress ahead of a blunted crack tip under small scale yielding (SSY) conditions. The tensile stress reaches a maximum value ($\sim(1+\pi/2)\sigma_0$) at a distance of $\sim 2 \times$ CTOD, where CTOD $\sim K^2/E$. The material is plastically deformed over a distance PZ $\sim 1/(3\pi) \times (K/\sigma_0)^2$ (plane strain). The HRR field [11,12] describes the variation of the tensile stress in the plastic zone beyond the maximum stress. The elastic field is also represented. Position of grains and initiation sites (an identified site is shown in the insert) are schematically indicated.

Fig. 3. Représentation schématique de la distribution de la plus grande contrainte principale en tête d'une fissure émoussée sous l'effet du chargement. La plasticité est confinée à la pointe de la fissure (SSY). La contrainte de traction est maximale ($\approx(1+\pi/2)\sigma_0$) à une distance d'environ deux fois le CTOD où CTOD $\sim K^2/E$. Le matériau en pointe de fissure est déformé plastiquement sur une distance PZ $\approx 1/(3\pi) \times (K/\sigma_0^2)$ (en déformation plane). Le champ HRR [11,12] décrit la variation de la contrainte de traction au-delà du maximum. Le champ élastique ($K/\sqrt{r}$) est également représenté. La position des grains et des sites d'amorçage du clivage (voir illustration dans l'encadré) est également montrée.

on Fig. 3. The maximum tensile stress, $\sigma_{yy}^{\mathrm{Max}}$ is of the order of $(1+\pi/2)\sigma_0$ and is thus equal to approximately three times the yield strength. This distribution of the tensile stress in the presence of a macroscopic crack suggests that fracture is not initiated from the crack tip but at sites located within the material ahead of the crack tip, as schematically shown in Fig. 3. Of course this analysis which is based on continuum mechanics applies only when the critical CTOD is much larger that the grain size. Otherwise crystal plasticity must be considered, as shown later.

The article is organised as follows: After this brief introduction, the micromechanisms of cleavage fracture in steels containing second phase particles are described in more detail, firstly qualitatively and then more quantitatively in order to present a model which is able to account for the characteristics of brittle cleavage fracture indicated previously. The mechanical basis of this model relies on continuum mechanics and the source of scatter is only related to the initiation sites. This approach has some limitations, in particular when crack tip plasticity extent is comparable to the grain size. This is the reason why the statistical origins of cleavage fracture related to the polycrystalline nature of the materials is discussed in a separate part. The application of this theoretical model to the prediction of Charpy impact test results is shown in the last part.

2. Cleavage micromechanisms and modelling

2.1. Qualitative description

In many structural steels, in the range of temperature where fracture is purely brittle, the mean cleavage stress, $\bar{\sigma}_c$, has been shown to be independent of temperature, as stated earlier. This suggests that in these materials the mechanism of cleavage fracture is *growth controlled*. In bainitic steels considered in this paper, cleavage microcracks are progressively nucleated from different microstructural features (particles, inclusions, colonies of carbides, etc.) under the influence of the plastic strain applied to the material ahead of a macroscopic crack tip. These microcracks are eventually arrested at microstructural barriers (see Fig. 4a and b), such as grain boundaries or packet boundaries whose nature and strength are strongly dependent of the microstructure considered. Fracture occurs when the longest microcrack reaches the Griffith stress given by $\sigma_c = \sqrt{2E\gamma_s/\alpha a}$, where a is the size of a microcrack, γ_s the *effective* surface energy and α a numerical constant related to the shape of the fractured defect. In this relation all the terms are almost independent of temperature, γ_s which is much higher than the true surface energy because of plasticity accompanying crack propagation can be also considered temperature independent within a first approximation. In the lower shelf of the DBT (ductile to brittle transition), this relation combined with a decrease of the maximum tensile stress with temperature predicts an increase of the fracture toughness with temperature.

However, this theory is too simple since it does not recognize the different steps encountered during microcrack nucleation and microcrack propagation.

Cleavage fracture in ferritic steels is related to microcracks initiation from brittle second-phase particles, for example carbides or nonmetallic inclusions, such as manganese sulfides, MnS, or titanium nitrides, TiN (see e.g. inserts in Figs. 3, 4a and 6). Cleavage fracture is a sequential process of elementary events: a cleavage microcrack initiated from the slip-induced cracking of a brittle particle can propagate dynamically within the adjacent ferrite, and then propagates into the neighbouring ferrite grains if the local arrest fracture toughness is not high enough as schematically illustrated in Fig. 3.

The first event, *the nucleation step*, corresponding to brittle fracture of particles, is governed by a critical stress, σ_n, when particle size is larger than 0.1–1 μm [13] which is approximately the case of the measured carbide size distribution for pressure vessel steels (see Fig. 5). Below this size, a dislocation-based theory must be used. It has been shown that the nucleation stress for 0.1–1 μm, σ_n, is related to the maximum principal stress, σ_1, the equivalent von Misès stress, σ_{eq} and the yield stress, σ_0, by:

$$\sigma_n = \sigma_1 + \lambda(\sigma_{eq} - \sigma_0) \tag{1}$$

where λ is a function of particle shape. The increase of strain (2nd term in Eq. (1)) needed to nucleate a microcrack with temperature as well as the effect of stress state conditions (1st term in Eq. (1)) on the increase of crack nucleation sensitivity is clearly shown by this relation. Full details can be found in [13]. Values of σ_n are statistically distributed as considered by several authors (see e.g. [14]). Nucleation step was not considered critical in most of the pioneering cleavage models. However particle induced cleavage microcracks nucleation may be a critical step depending on the microstructure, the constraint, the amount of plastic strain, the temperature and the loading path as shown by several authors (see e.g. [15,16]).

During the first steps of microcrack propagation, microstructural barriers as bainitic lath packets or grain boundaries may deviate or arrest the cleavage microcracks as shown in Fig. 4b or evidenced by acoustic emission [17]. It has been shown recently that in bainitic steels the crack arresting boundaries are those for which the misorientation between the bainite packets is large [9,17]. The character of the grain boundaries (tilt or twist) is critical as shown in Fig. 4c where local crack front deviations and crack fragmentation are observed. This qualitative description suggests that multiple barriers models including various length scales must be developed.

2.2. Statistical effects related to microstructural defects distribution

The first characteristic of brittle fracture in ferritic steels is the scatter of the test results. Most existing probabilistic models consider crack nucleation as being secondary in importance and base their development upon the assumption that macroscopic failure occurs when the local macroscopic applied stress is sufficient to propagate pre-existing microcracks through the body. Once the propagation is started, the energy spent over the whole propagation up to the final fracture is not taken into account in these approaches.

Pioneering studies have then related the statistical variation in K_{IC} values to the size distribution of particles which initiate cleavage microcracks, thus assuming the pre-existence of the distribution of cracked particles in the material and its equivalence to the particle size distribution. To simplify the proposed models it was also assumed that the nature, as well as the size distribution of the microstructural defects, remain identical with straining and over the temperature range where brittle fracture is observed.

The microcrack size distribution induces a statistical distribution of local fracture stresses based on the Griffith's theory [18]. This has been the basis of the development of statistical modelling of cleavage fracture as proposed in the pioneering work of Beremin group [19] and Wallin [20]. Assuming that the size distribution of microdefects is described

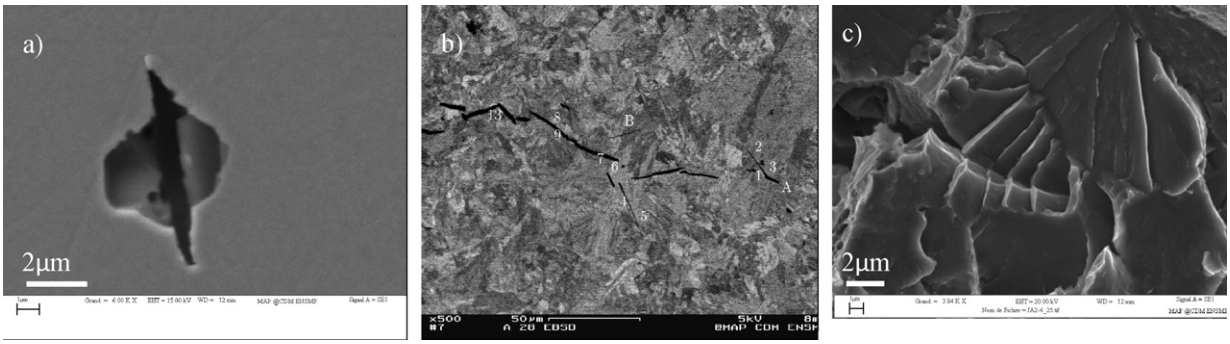

Fig. 4. Cleavage microcrack propagation arrest related to microstructural misorientations. a) Cleavage microcrack nucleated from a particle (MnS inclusion) and arrested in the surrounding matrix. 16MND5 steel, test temperature: −120 °C [10]; b) Secondary cleavage microcracks located below the main cleavage crack, deviated or arrested by microstructural barriers. 16MND5 steel, test temperature −100 °C [10]; c) Details of grain boundary crossing by cleavage cracks (16MND5 steel).

Fig. 4. Illustration des phénomènes d'amorçage et d'arrêt de microfissures de clivage liés à la microstructure. a) Microfissure de clivage amorcée à partir d'une inclusion de sulfure de manganèse et arrêtée dans la ferrite – Acier 16MND5. Température d'essai = −120 °C [10] ; b) Microfissures de clivage secondaires observées sous la surface d'une fissure principale. Noter l'arrêt ou la déviation de ces microfissures à des joints fortement désorientés – Acier 16MND5. Température d'essai = −100 °C [10] ; c) Faciès d'une surface de rupture montrant la fragmentation du plan de clivage à la traversée des joints de grain.

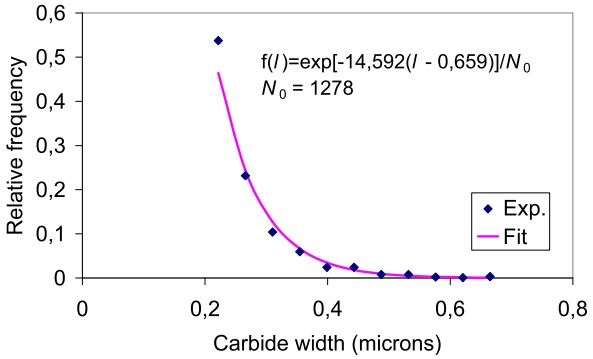

Fig. 5. Carbide width probability distribution function in a low alloy pressure vessel steel [15].

Fig. 5. Distribution de la taille des particules de carbures dans un acier pour réacteur à eau sous pression [15].

by a simple (power or exponential) law, $g(a)$, the weakest link theory writes that the probability to failure $p(\sigma)$ of a representative elementary volume element, V_u, is given by:

$$p(\sigma) = \int_{a_c(\sigma)}^{\infty} g(a)\,\mathrm{d}a \tag{2}$$

where $a_c = 2E\gamma_s/\alpha\sigma_c^2$. Under the weakest assumption, the failure probability of a volume V, P_R, can then be easily derived. The main difficulty is then to assess the distribution function $g(a)$. When the critical step for cleavage fracture is the propagation of microcracks initiated from particles (carbides, inclusions, martensite–austenite constituents, etc.) which can be metallographically observed, the distribution $g(a)$ can be determined experimentally. Two types of laws have been proposed from these observations: the power law and the exponential law (see e.g. [21]). An exponential law describing the (M_2C or M_3C type) carbides width distribution for low alloy pressure vessel steel is illustrated in Fig. 5 where it is shown that all dimensions are submicronic.

This distribution can be approximated by a power law $g(a) = \kappa a^{-\beta}$. This leads to the well-known Weibull expression which has been successfully used to describe the probability to failure of brittle materials (see e.g. [22]). Assuming that microcracks propagation is controlled by the maximum principal stress, σ_I, and that nucleation is controlled by microplasticity activity, the Beremin group has proposed the following expression for the failure probability:

$$P_R^B = 1 - \exp\left[-\frac{\int_{V_p} \sigma_I^m \frac{\mathrm{d}V}{V_u}}{\sigma_u^m}\right] \tag{3}$$

where the mth-root of the integral term is known as the "Weibull stress", σ_W, and the volume integral is extended over the whole plastic zone, V_p. The Weibull shape factor is given by $m = 2\beta - 2$ and the normalizing factor is given by

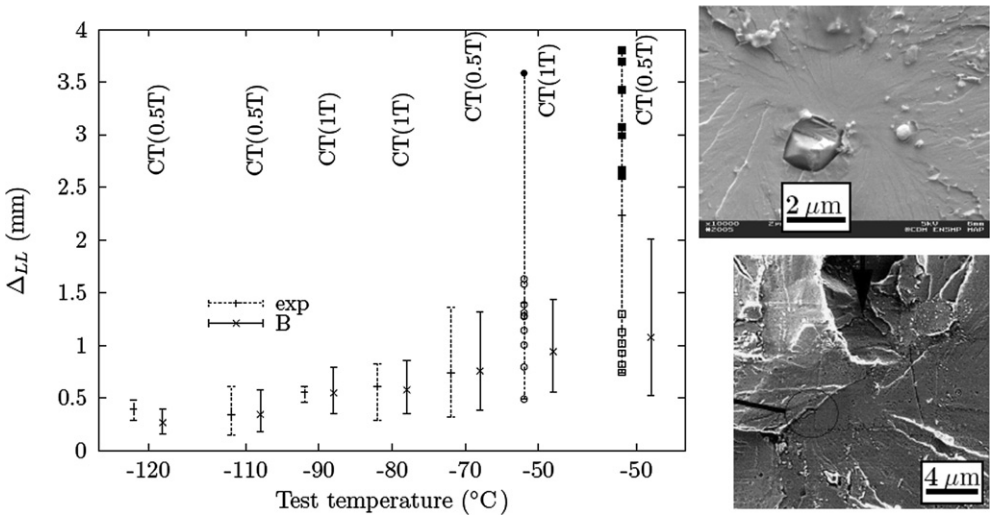

Fig. 6. 16MND5 pressure vessel steel. Comparison between experimental (exp) load line displacement at fracture and corresponding predictions by Beremin model (B) for a failure probability of 5% and 95%. At −50 °C, each experiment is represented by a symbol. The full symbols correspond to experiments where ductile crack precedes cleavage initiation. Micrographs on the right side of the figure correspond to examples of microstructural features identified at the origin of cleavage fracture triggering. CT: compact tension specimen; XT: specimen thickness in inches [2].

Fig. 6. Acier 16MND5. Déplacement à diverses températures de la ligne d'application de la charge à rupture mesuré (exp) et prédit par le modèle de Beremin (B) pour des probabilités à rupture de 5 % et 95 %. A −50 °C, le résultat de chaque expérience est représenté par un symbole. Les symboles pleins correspondent à des expériences au cours desquelles la rupture par clivage est précédée par une propagation ductile. Les fractographies à droite illustrent des exemples de sites d'amorçage. CT : Eprouvette « *Compact Tension* » ; XT : Epaisseur des éprouvettes en pouces [2].

$\sigma_u = (m/2\kappa)^{1/m}(2E\gamma_s\alpha)^{1/2}$. From this last relation, one can inferred that σ_u which is interpreted as the cleavage stress of a representative volume is dependent on the *effective* surface energy but also on the distribution of defects involved in cleavage fracture process. It should be pointed out that the statistical distribution is different from the Weibull law when the probability distribution function of the defects is described by an exponential law. The statistical distribution is then given by a double exponential law, which is a Gumble type function.

The concept of Weibull stress has been extended to situation where the material located ahead of the crack tip is not macroscopically homogeneous (functionally graded materials, welds, etc.) (see e.g. [23,24]). This concept is now used in the ISO standards to transfer the results of laboratory tests to components [25].

Application of expression (3) to the crack tip situation is straightforward under small scale yielding (SSY) assumption. The probability distribution for the fracture toughness of a specimen, containing a 2D macrocrack, scaled in terms of K_{Ic}, can be written as:

$$P_{\mathrm{R}}^{\mathrm{B}} = 1 - \exp\left[-\frac{K_{\mathrm{IC}}^4 B_f \sigma_0^{m-4} C_m}{\sigma_u^m V_u}\right] \tag{4}$$

where B_f is the crack front length, and C_m is a numerical factor which is an increasing function of the work-hardening exponent of the material. For a given probability to fracture, Eq. (4) can be expressed by the following relation $\sigma_0^{m-4} K_{\mathrm{Ic}}^4 B_f =$ cst from which the prediction of the size effect illustrated in Fig. 1 is clearly shown.

Eqs. (3) and (4) have been applied in many studies in order to predict the fracture toughness of low alloy pressure vessel steels within the lower part of the DBT range. Comparison between predictions obtained from Eq. (3) and experimental results [2] are reported in Fig. 6. In this figure, the scatter predicted by Beremin model corresponding to a failure probability of 5% and 95% is compared to load line displacement at fracture values obtained from two different sizes of fracture mechanics specimens. Besides the rather good capacity for predicting the scatter in tests results at temperatures between −120 °C and −70 °C, it is shown that the test results scatter increases at higher temperature. This is partly related to the initiation and propagation of a ductile crack before cleavage fracture. In these conditions the simple analytical expression given by Eq. (4) (which is valid only for small scale yielding) cannot be strictly applied. In the presence of ductile crack growth preceding cleavage fracture a numerical simulation including both types of models (ductile (see e.g. Pardoën, in this issue) and cleavage) must be used. Very few authors have attempted to model this situation observed in the ductile-to-brittle transition. However, a number of references can be found elsewhere [26].

2.3. A further understanding of statistical origin of cleavage fracture due to local stress–strain inhomogeneities

As stated earlier, the statistical distribution of local fracture stresses which are directly related to cleavage micromechanisms are experimentally determined from microstructural observations. Another source of scatter is related to the statistical

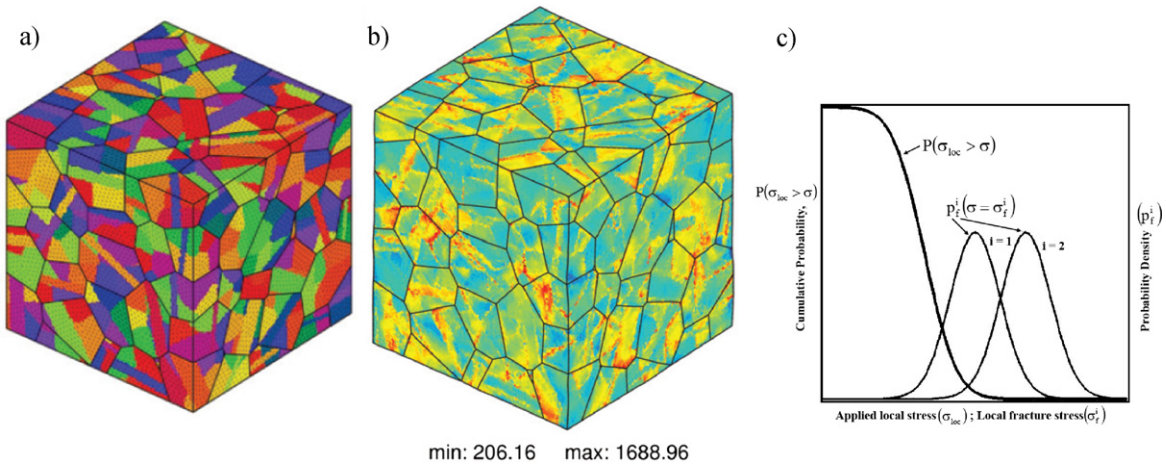

Fig. 7. Finite Element simulations at representative elementary volume scale based on polycrystalline plasticity. a) Simulation of the initial microstructure; b) Von Misès equivalent stresses distribution for an aggregate with packets ISO + NW [32]; c) Schematic calculations of the probability of failure when the cumulative probability of local applied stress, $P(\sigma_{loc} > \sigma)$, is distributed, and when the probability densities of local fracture stresses $p_f^i(\sigma > \sigma_f^i)$ are known. Two micromechanisms are considered $(i = 1, 2)$ [27].

Fig. 7. Simulation de la plasticité polycristalline par éléments finis à l'échelle d'un élément de volume représentatif. a) Microstructure initiale ; b) Distribution de la contrainte de von Mises dans un agrégat comportant des paquets ISO + NW [32] ; c) Principe de calcul de la probabilité de rupture quand on connaît la probabilité cumulée des contraintes à rupture locales, $p(\sigma_{loc} > \sigma)$ et quand les densités de probabilité des contraintes à rupture locales, $p_f^i(\sigma > \sigma_f^i)$ sont également connues. Deux mécanismes de rupture sont envisagés $(i = 1, 2)$ [27].

distribution of the local applied stresses which is linked to the orientation of the grains within a polycrystal. This orientation effect arises from the anisotropy in elasticity and mainly in plasticity.

The inhomogeneous stress distribution in polycrystals in relation with crystalline elastic anisotropy has been studied by several authors (see e.g. [27]). Pommier [28] showed numerically that even in randomly oriented polycrystals the local stresses in a given grain are related to those existing in neighboring grains. The stresses in a polycrystal are thus arranged in a network whose scale is larger than the grain size. The representative elementary volume (REV) is therefore larger than the grain size and is related to the size of the percolation network. This corresponds to a situation similar to that encountered in granular materials and to "arching" effect observed in these materials. Kotrechko [29] and Gurev [30] have also investigated the effect of elastic anisotropy. These authors have proposed a relationship between the microscopic elastic stresses, σ_{ij}^m, acting within a grain and the macroscopic principal stresses $(\sigma_1, \sigma_2, \sigma_3)$. The variance of σ_{ij}^m has also been calculated as a function of elastic anisotropy coefficients. In randomly oriented polycrystalline iron loaded in tension along the direction 1, σ_{11}^m varies in a range from $0.6\sigma_1$ to $1.4\sigma_1$ (for a standard deviation of ± 3 s), while the values of σ_{22}^m and σ_{33}^m vary from $-0.24\sigma_1$ to $0.24\sigma_1$.

The analysis of plastic crystalline solids using homogenization technique or Finite Element (FE) simulations is becoming more and more classical in the literature, see e.g. [31,32] for a comprehensive review. This FE approach has been largely applied to FCC polycrystals and, more recently, to a BCC steel with a bainitic structure [33]. The crystallographic orientations of the bainitic packets were assumed to be either randomly distributed (ISO) or oriented with respect to the prior austenite grains, according to the Nishiyama–Wasserman relationship [NW] (Fig. 7a), i.e.:

$$(111)_\gamma \parallel (011)_\alpha \quad \text{and} \quad [\bar{1}2\bar{1}]_\gamma \parallel [\bar{1}\bar{1}1]_\alpha$$

The Kurdjumov–Sachs orientation relationship was also considered. One "picture" illustrating the results obtained from these numerical simulations is shown in Fig. 7b. This figure illustrates the wide distribution in local stresses, σ_{loc}, which can be as large as the macroscopic mean stress.

This distribution in local stresses can also contribute to the scatter in the measurement of cleavage stress. Knowing this distribution and that of the local fracture stresses, it is then theoretically possible to calculate the probability to fracture, P_R, using the weakest link concept, as schematically indicated in Fig. 7c. Assuming that the REV corresponding to σ_{loc} is larger than the REV associated with a given fracture event (carbides, grain boundary), the probability to fracture can be written as:

$$P_R = \int_o^\infty P(\sigma_{loc} > \sigma) \times p_f^i\left(\sigma = \sigma_f^i\right) d\sigma \tag{5}$$

where $p_f^i(\sigma = \sigma_f^i)$ is the probability density of local fracture stresses corresponding to the event i. It should be added that in the presence of successive microstructural barriers, conditional probability expressions must be used to calculate the probability to fracture (see e.g. [17]).

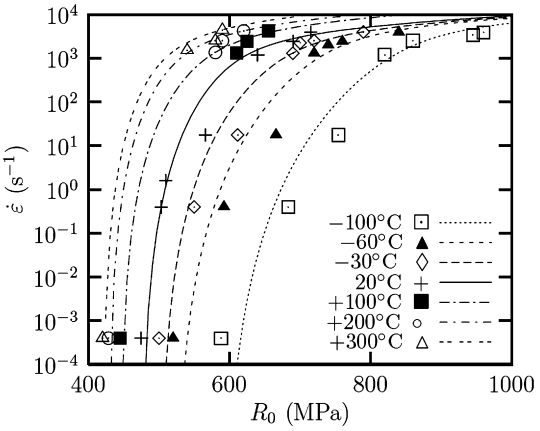

Fig. 8. 16MND5 steel. Variation of yield stress, R_0, with strain rate and temperature [10].

Fig. 8. Acier 16MND5. Variation de la limite d'élasticité, R_0, avec la vitesse de déformation et la température [10].

This approach can account for another source of scatter related to the crystallographic aspect, i.e. the value of the shape factor parameter, m, in the Weibull distribution and its potential temperature dependence. However this approach cannot be easily used in the presence of a macroscopic crack where they are large stress and strain gradients. This is the reason why it is felt that the simplified Beremin model will remain practically largely used still for a long time. It should be added that both type of approaches still remain relatively macroscopic. Local stresses must be known at a smaller scale, that of slip lines and dislocation pile-ups. This is especially true in pure metals as indicated earlier in the Introduction.

3. Application to nuclear pressure vessel structural integrity

The Charpy V or CVN impact test remains the most convenient and the most widely method used to determine the fracture properties of ferritic steels. In most countries the surveillance program of nuclear reactor pressure vessel which aims at monitoring the embrittlement due to irradiation is based on Charpy V impact curve and his shift towards higher temperature with increasing exposure to neutron irradiation. In this technological test, a notched specimen is impacted by a hammer at a velocity of about 5 m/s. Classically the absorbed energy, the shear fracture appearance (SFA) and the lateral expansion are measured. However the considered energy-based temperature index used in the surveillance programs ignores the underlying mechanisms of crack formation, propagation and arrest so that a direct and robust correlation between fracture toughness and impact energy cannot be simply derived. Developments in the local approach to fracture have evolved the Charpy V impact test from a quality control test to an evaluation tool for structural integrity assessment of materials.

Modelling the Charpy test is a difficult task, since several aspects of this test require a detailed analysis: the inertial effects, the complexity of the loading and the boundary conditions, the effect of large strains and high strain rates on constitutive equations, the quasi-adiabatic character of the test, the 3D character of fracture behaviour, in particular ductile crack growth preceding cleavage fracture above the lower-shelf temperature and the competition between ductile and brittle fracture. A finite simulation of the Charpy test has been proposed in few studies [10,34,35] in order to simulate the DBT curve. This is briefly illustrated using the results of a study performed on a RPV A508 steel. A full account of the results can be found elsewhere [36,37]. In this study a special effort was undertaken in order to characterize and to introduce in the constitutive equations the sensitivity of the yield stress to the strain rate at different temperatures. The evolution of the yield stress over a wide range of strain rate and temperature is represented on Fig. 8. Several laws have been proposed in the literature in order the represent the strain rate dependence of yield strength in mild and ferritic steels [38,39].

In [10], an inverse double Norton law has been proposed to represent continuously the yield stress variation, with strain rate, $\frac{1}{p} = \frac{1}{\dot{\varepsilon}_1} + \frac{1}{\dot{\varepsilon}_2}$ with $\dot{\varepsilon}_i = \langle \frac{\sigma - R}{K_i} \rangle^{n_i}$ where σ is the tensile stress and R the flow stress of the material which is a function of temperature and plastic strain, K_i and n_i $(i = 1, 2)$ are material coefficients. Each "component" of the strain rate, $\dot{\varepsilon}_1$ and $\dot{\varepsilon}_2$, is representative of a deformation mechanism: (1) Peierls friction; (2) phonon drag [38]. The mechanism with the smallest deformation rate controls deformation. A good agreement between proposed modelling (lines) and experiments (symbol) is observed in Fig. 8.

A first approach of the DBT is to consider ductile and brittle fracture as competitor failure mechanisms but weakly coupled: ductile crack growth modifies the stress–strain fields as well as the sampled material volume from which the cleavage triggering will be affected but do not modify the cleavage fracture micromechanisms themselves.

Ductile failure is commonly represented by models using a single damage parameter which represents the void volume fraction (for further details see Pardoen in this special issue). This approach has been shown to be efficient to represent the salient features of ductile damage in a Charpy specimen in particular the tunnelling crack front (see Fig. 9a), the correlation of ductile crack front length with absorbed Charpy energy, and the increase of maximum principal stress from a notch to

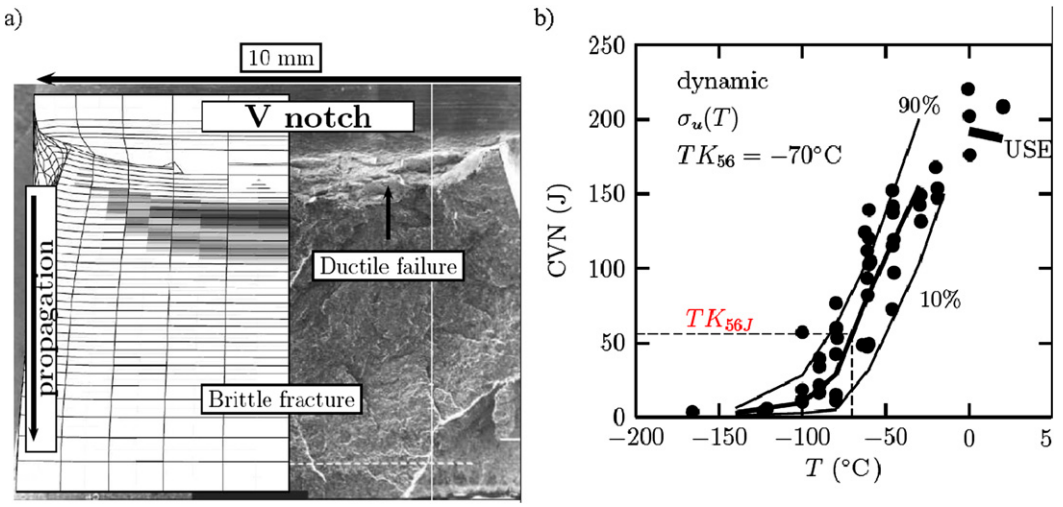

Fig. 9. Modelling Charpy energy curve using LAF [37]. a) Comparison between ductile crack propagation obtained from modelling and experiments; the maximum principal stress location ahead of the ductile crack controlling the cleavage triggering is represented in grey levels; b) Prediction of the Charpy toughness transition curve.

Fig. 9. Modélisation de la courbe de transition Charpy à l'aide de l'approche locale de la rupture (LAF) [37]. a) Comparaison entre le modèle et l'expérience montrant l'avancée de fissure ductile avant l'apparition du clivage. La position de la plus grande contrainte principale contrôlant le clivage est indiquée en niveau de gris ; b) Prévision de la courbe de transition.

a propagating ductile crack [10,37]. However at the considered scale, local effects as heterogeneous spatial damage ahead of the main ductile crack front or corrugated crack front are not represented, even tough there are presumed to play a potential role in the observed scatter inherent to the DBT.

Brittle fracture is described using the Beremin model (Eq. (3)) modified in order to take into account the unloading of the material left behind the crack front during ductile crack growth (see further details in [37]). Fig. 9 shows the comparison between an experimental fracture surface exhibiting the ductile fracture zone initiated from the notch, the cleavage fracture and the contour plots of the maximum principal stress. The observed tunnelling effect is well reproduced and the location of the maximum principal stress ahead of the crack front is in agreement with the experimentally identified cleavage initiation sites from fractographic investigations. Fig. 9b reports the calculated energies corresponding to failure probabilities of 10%, 50% and 90% and the experimental results. It is shown that a good description of the whole DBT range is obtained providing a temperature dependence of the Beremin stress parameter σ_u (see Eq. (2)), whereas it was shown that a constant value of the parameter σ_u will lead to correct prediction of the reference temperature T_{K56J} but to a large underestimation of the CVN energies in the upper part of the DBT. The reasons of the apparent temperature dependence of the Beremin stress parameter σ_u are not yet fully understood. Modelling of cleavage fracture in the DBT is still investigated through the development of new models physically enriched at different scales: description of the nucleation and propagation mechanisms as conditional steps of cleavage fracture (see e.g. [15]) at continuum level, description of the heterogeneities of stress and strain field at grain scale.

4. Conclusions

- Linear and non-linear fracture mechanics are disciplines which have largely contributed to structural integrity assessment. However these approaches have a number of limitations, in particular the transferability of laboratory test results to components. This is the reason why the local approach to fracture (LAF) was developed in the 80s. This local approach has now largely contributed to the transferability of test results. In particular it can account for the scatter and size effect and load-temperature history effect observed in the brittle fracture regime.
- Significant improvements in the understanding and modelling of cleavage fracture have been made over the past twenty years. Modelling based on the distribution of microstructural effects has allowed reproducing the scatter and the size effect. Recent developments in the simulation of crystalline plasticity have been used for a better understanding of statistical aspects of cleavage fracture. A large research effort remains to be made for a better understanding of the temperature dependence of the *effective* surface energy or, similarly the *critical fracture stress*, σ_u, in the Beremin theory.
- The application of ductile fracture models combined with models for brittle fracture has reached a level of development which enables structural integrity assessments.
- Limitations of the existing models can be partly overcome through a more detailed description of the plasticity and damage at a lower scale.

Acknowledgements

Financial support from Ministry of Industry, EDF, CEA and AREVA is acknowledged. A.P. would like to thank all his PhD students who have been involved in this long-term research project.

References

[1] A. Pineau, Development of the local approach to fracture over the past 25 years: Theory and applications, Int. J. Fracture 138 (2006) 139–166.
[2] B. Tanguy, C. Bouchet, S. Bordet, J. Besson, A. Pineau, Towards a better understanding of the cleavage in RPV steels: Local mechanical conditions and evaluation of a nucleation enriched Weibull model and of the Beremin model over a large temperature range, in: 9th European Mechanics of Materials Conference, Moret-sur-Loing, France, 2006.
[3] A.N. Stroh, The formation of cracks as a result of plastic flow, Proc. R. Soc. Lond. A 223 (1954) 404–414.
[4] A.H. Cottrell, Theory of brittle fracture in steel and similar metals, Trans. AIME 212 (1958) 192–203.
[5] D. Hull, Twinning and fracture of single crystals of 3% silicon iron, Acta Met. 8 (1960) 11–18.
[6] J.F. Knott, Fundamentals of Fracture Mechanics, Butterworth, London, 1973.
[7] E. Smith, The nucleation and growth of cleavage microcracks in mild steel, in: Physical basis of yield and fracture, Oxford, 1966.
[8] T.C. Lindley, G. Oates, C.E. Richards, A critical appraisal of carbide cracking mechanisms in ferrite/carbide aggregates, Acta Metall. 18 (1970) 1127–1136.
[9] E. Bouyne, H. Flower, T. Lindley, A. Pineau, Use of EBSD technique to examine microstructure and cracking in bainitic steel, Scripta Materialia 39 (3) (1998) 295–300.
[10] B. Tanguy, Modélisation de l'essai Charpy par l'approche locale de la rupture. Application au cas de l'acier 16MND5 dans le domaine de la transition, PhD thesis, Ecole des Mines de Paris, 2001.
[11] J.W. Hutchinson, Plastic stress and strain fields at a crack tip, J. Mech. Phys. Solids 16 (1968) 337–347.
[12] J. Rice, G. Rosengren, Plane strain deformation near a crack tip in a power-law hardening material, J. Mech. Phys. Solids 16 (1968) 1–12.
[13] F. Beremin, Cavity formation from inclusions in ductile fracture of A508 steel, Met. Trans. A 12 (1981) 723–731.
[14] B.Z. Margolin, A.G. Gulenko, V. Shvetsova, Improved probabilistic model for fracture toughness prediction for nuclear pressure vessel steels, Int. J. Pressure Vessels and Piping 75 (1998) 843–855.
[15] S. Bordet, B. Tanguy, J. Besson, D. Moinereau, A. Pineau, Cleavage fracture of a RPV steel following warm pre-stressing: Microstructural analysis and interpretation through a new model, Fatigue Fract. Eng. Mater. Struct. 29 (9/10) (2006) 799–816.
[16] S.R. Yu, Z.G. Yan, R. Cao, J.H. Chen, On the change of fracture mechanism with test temperature, Eng. Frac. Mech. 73 (2006) 331–347.
[17] A. Lambert-Perlade, A.-F. Gourgues, J. Besson, T. Sturel, A. Pineau, Mechanisms and modelling of cleavage fracture in simulated heat-affected zone microstructure of a high strength low alloy steel, Metall. Mater. Trans. A 35 (2004) 1039–1053.
[18] A.A. Griffith, The phenomena of rupture and flow in solids, Phil. Trans. A 221 (1920) 163–198.
[19] F. Beremin, A local criterion for cleavage fracture of a nuclear pressure vessel steel, Met. Trans. A 14 (1983) 2277–2287.
[20] K. Wallin, T. Saario, K. Törrönen, Statistical model for carbides induced brittle fracture in steel, Metal Science 18 (1984) 13–16.
[21] B. Tanguy, J. Besson, A. Pineau, Comment on effect of cardide distribution on the fracture toughness in the transition region of an SA 508 steel, Scripta Materialia 49 (2003) 191–197.
[22] R. Danzer, P. Supansic, J. Pascual, T. Lube, Fracture statistic of ceramics – Weibull statistics and deviation from Weibull statistics, Eng. Frac. Mech. 74 (2007) 2919–2932.
[23] T.L. Becker, R.M. Cannon, R.O. Ritchie, Statistical fracture modeling: Crack path and fracture criteria with application to homogeneous and functionally graded materials, Eng. Frac. Mech. 69 (2002) 1521–1555.
[24] B. Bezensek, J.W. Hancock, The toughness of laser welded joints in the ductile–brittle transition, Eng. Fract. Mech. 74 (2007) 2395–2419.
[25] ISO-27306, Method of constraint loss correction of CTOD fracture toughness assessments of steel components, 2009.
[26] A. Pineau, Modelling ductile to brittle fracture transition in steels – Micromechanical and physical challenges, Int. J. Fracture 150 (2008) 129–156.
[27] A. Pineau, Statistics of brittle cleavage fracture in steels, in: CMDS 11, Mines Paris ParisTech, 2008, in press.
[28] S. Pommier, Arching effect in elastic polycrystals: Implications for the variability of fatigue lives, Fatigue Fract. Eng. Mater. Struct. 25 (2002) 331–348.
[29] B. Kotrechko, B. Strnadel, I. Dlouhy, Fracture toughness of cast ferritic steel applying local approach, Theor. Appl. Fract. Mech. 47 (2007) 171–181.
[30] A.V. Gurev, E.P. Bogdanov, Effect of structural stresses on the strength of polycrystalline materials, Strength Mater. 16 (1984) 81–87.
[31] F. Barbe, L. Decker, D. Jeulin, G. Cailletaud, Intergranular and intragranular behavior of polycrystalline aggregates. Part 1: F.E. model, Int. J. Plasticity 17 (2001) 513–536.
[32] F. Barbe, L. Decker, D. Jeulin, G. Cailletaud, Intergranular and intragranular behavior of polycrystalline aggregates. Part 2: Results, Int. J. Plasticity 17 (2001) 537–563.
[33] N. Osipov, A.-F. Gourgues-Lorenzon, B. Marini, V. Mounoury, F. Nguyen, G. Cailletaud, FE modelling of bainitic steels using crystal plasticity, Philos. Mag. 88 (2008) 3757–3777.
[34] W. Schmitt, D. Sun, W. Böhme, G. Nagel, Evaluation of fracture toughness based on results of instrumented Charpy tests, Int. J. Pressure Vessels and Piping 59 (1994) 21–29.
[35] A. Rossoll, Détermination de la ténacité d'un acier faiblement allié à partir de l'essai Charpy instrumenté, PhD thesis, Ecole Centrale Paris, 1998.
[36] B. Tanguy, J. Besson, R. Piques, A. Pineau, Ductile to brittle transition of an A508 steel characterized by the Charpy impact test. Part I: Experimental results, Eng. Frac. Mech. 72 (1) (2005) 49–72.
[37] B. Tanguy, J. Besson, R. Piques, A. Pineau, Ductile to brittle transition of an A508 steel characterized by the Charpy impact test. Part II: Modelling of the Charpy transition curve, Eng. Frac. Mech. 73 (3) (2005) 413–434.
[38] J. Campbell, W. Ferguson, The temperature and strain-rate dependence of the shear strength of mild steel, Philos. Mag. 21 (1970) 63–82.
[39] J.B. Lean, J. Plateau, C. Crussard, Etude des propriétés mécaniques et de la rupture fragile de l'acier doux, C. R. Acad. Sci. 247 (1958) 306–309.